Evidence for Sub-picosecond Heme Doming in Hemoglobin and Myoglobin: A Time-Resolved Resonance Raman Comparison of Carbonmonoxy and Deoxy Species†

S. Franzen,‡ B. Bohn,§ C. Poyart,§ and J. L. Martin*,‡

Laboratoire d'Optique Appliquée, INSERM U275, Ecole Polytechnique-ENSTA, 91120 Palaiseau, France, and INSERM U299, Le Kremlin-Bicetre, France

Received February 1, 1994; Revised Manuscript Received November 8, 1994⊗

ABSTRACT: Separation of the photophysical aspects of the sub-picosecond (sub-ps) time-resolved resonance Raman signal from contributions due to conformation has been achieved by comparing deoxyhemoglobin (Hb) in the T state with (carbonmonoxy)hemoglobin (HbCO), deoxy-β_4 (β_4CO) (all R state), and monomers deoxymyoglobin and (carbonmonoxy)myoglobin (MbCO) [β_4 consists of a tetramer of four β-subunits and shows no cooperativity]. In all photolyzed species, Hb*(CO), Mb*(CO), and β_4*(CO), the iron-histidine out-of-plane mode (ν_{Fe-His}), indicative of heme doming, achieves 90% of its full intensity in 1 ps. The frequency of this mode (223−228 cm^{-1}) is shifted significantly relative to equilibrium deoxy-Hb (210−216 cm^{-1}) in the T state, but not with respect to either equilibrium deoxy-Mb or deoxy-β_4. A correlation between the +12 cm^{-1} bandshift of ν_{Fe-His} and the −2 cm^{-1} shift of the electron density marker band (ν_4 at 1370 cm^{-1}) relative to T-state deoxy-Hb is shown to hold on all time scales, including the sub-picosecond time scale. Photolyzed Hb*(CO) consists of R-state or weakly interacting tetramers on the picosecond time scale and is shown to have properties similar to those of photolyzed Mb*(CO) and β_4*(CO) on the picosecond time scale. These results establish that heme doming occurs as an ultrafast reaction to ligand dissociation and that heme doming is the primary event in the sequence of conformational changes leading to the cooperative R → T transition.

In the oxygen transport protein hemoglobin, the formation or breakage of a single chemical bond between the heme iron and a diatomic ligand is transmitted to the protein and expressed in terms of intersubunit structural changes, which ultimately modify the binding affinity of all four heme irons in the protein. The X-ray crystal structure of hemoglobin shows that the heme iron is nearly coplanar with the heme in ligated hemoglobin and more than 0.4 Å from the heme plane in deligated hemoglobin (Perutz, 1979). The out-of-plane iron displacement or heme doming, which results from the breaking of the iron−ligand bond, is thought to initiate the series of conformational changes that ultimately leads to a quaternary structure change, inducing cooperative behavior among the heme iron binding sites in hemoglobin (Perutz, 1970; Baldwin & Chothia, 1979).

Hemoglobin is known to undergo a cooperative transition from a relaxed state, R, with high affinity for a diatomic ligand, such as O_2, CO, or NO, to a tense state, T, with low ligand binding affinity. The R → T transition is a quaternary transition that occurs on the microsecond time scale following ligand photodissociation (Sawicki & Gibson, 1976; Hofrichter et al., 1983). Prior to the quaternary transition, there are changes in tertiary structure over a range of time scales from picosecond to microsecond. Time-resolved resonance Raman (TRRR) spectroscopy has played an important role in measuring the time scale of these structural changes and elucidating specific models of the reaction coordinate (Scott & Friedman, 1984).

In the high-frequency region of the resonance Raman (RR) spectrum of Hb, the electron density marker, or ν_4 Raman band, observed at 1355 cm^{-1} in deoxy Hb exhibits a time-dependent shift in photodissociated HbCO (denoted Hb*-(CO) or simply Hb*). The time scale of relaxation of the ca. −2 cm^{-1} ν_4 bandshift to the equilibrium deoxy-Hb frequency has been used to estimate the time scale of tertiary and quaternary structural changes in Hb* that result in the formation of deoxy-Hb in the T state (Friedman et al., 1982a). In the low-frequency region of the RR spectrum, it has been shown that the Fe−His out-of-plane mode, ν_{Fe-His}, is absent from HbCO, but appears at a shifted position of 223−228 cm^{-1} in photolyzed (R state) HbCO as measured at 30 ps and 10 ns, later relaxing to the equilibrium (T state) deoxy position of 210−216 cm^{-1} on the 100 ns to microsecond time scale (Scott & Friedman, 1984). It has been shown that the frequencies of ν_{Fe-His} in the α- and β-subunits of T-state hemoglobin are 203 and 220 cm^{-1}, respectively; the R-state values are nearly the same at 223 and 224 cm^{-1} (Nagai & Kitagawa, 1980). This suggests that the single value of 212−216 cm^{-1} reported in this paper and elsewhere is the average of the value obtained in the different subunits. Studies have established that the ν_{Fe-His} mode is indicative of a domed heme (Nagai & Kitagawa, 1980; Argade et al., 1984).

Heme doming has been hypothesized to be the primary event in the series of conformational changes responsible for the cooperative R → T transition in hemoglobin (Perutz, 1970). At first this hypothesis was based on the correlations between quaternary structure and heme iron position (and

† S.F. was the recipient of a European Molecular Biology Organization fellowship.
‡ INSERM U275.
§ INSERM U299.
⊗ Abstract published in *Advance ACS Abstracts,* January 1, 1995.

0006-2960/95/0434-1224$09.00/0

spin state). One-color picosecond TRRR spectroscopy has been used to show that heme iron doming occurs on the time scale of 25 ps or less (Findsen et al., 1985b). Mounting evidence from transient absorption studies and molecular dynamics simulations suggests that heme doming occurs on the sub-picosecond time scale (Martin et al., 1983a,b; Henry et al., 1985; Kuczera et al., 1990; Lim et al., 1993; Gibson et al., 1992). An ultrafast heme iron conformational change could have two important consequences for the function of the molecule: (1) as a mechanism to prevent rapid ligand rebinding and (2) in the transduction of the rupture of a single chemical bond into a mechanical motion involving entire α-helices and, ultimately, the reorientation of subunits.

In the present study, we report an extension of the time resolution of the entire Raman spectrum from 200 to 1700 cm^{-1} to less than 1 ps using a two-color time-resolved resonance Raman experiment. In order to demonstrate sub-picosecond heme doming using TRRR spectroscopy by flash photolysis, it is necessary to separate the effects of excitation on the electronic and vibrational states of the heme from those due to conformational changes (Petrich et al., 1987). By comparing the TRRR signals of deoxyhemoglobin (Hb), deoxymyoglobin (Mb), (carbonmonoxy)hemoglobin (HbCO), and (carbomonoxy)myoglobin (MbCO), we demonstrate separation of the effects due to heme photophysics from those due to conformational changes on the picosecond (ps) time scale. As further proof of differences between cooperative and non-cooperative globins, we present comparisons between HBA consisting of two α-subunits and two β-subunits and non-cooperative β_4 globin, which consists of four β-subunits. It will be shown that the conformationally unrelaxed R state (and heme photophysics) in Hb*(CO) is virtually identical to those in Mb*(CO) and β_4*(CO) on the picosecond time scale. This result establishes the fact that the subunits of Hb behave like isolated monomers on the picosecond time scale. The conformational changes that give rise to cooperativity in hemoglobin are well separated in time from the initial event, heme doming. The data presented here prove that the initial displacement of the iron out of the heme plane following ligand photodissociation occurs on the sub-picosecond time scale.

MATERIALS AND METHODS

Sample Preparation

HbA (human adult) was prepared from fresh blood cell hemolysates withdrawn from healthy nonsmoking donors. HbA was isolated and purified by chromatography on a DEAE-Sephadex column. The purity of the solute was verified by isoelectric focusing, showing a single band migrating at $pI = 6.95$. The hemoglobin was further stripped of remaining contaminants on an ion-exchange column consisting of ion-retardation resin AG 11A8 and mixed-bed exchange resin AG 501X8-D from Bio-Rad. Hemoglobin was concentrated under vacuum to 2 mM heme and stored in the oxy form in liquid nitrogen until use. The methemoglobin content of the stock was less than 2%. Deoxyhemoglobin was prepared from the stock by equilibration under a stream of argon in 100 mM phosphate buffer (pH 7) at room temperature. The completeness of the deoxygenation was evaluated by spectrophotometry. The methemoglobin content of the solutions was less than 3%. Lyophilized horse heart metmyoglobin type III (batch M-1882, Sigma Chemical Co., St. Louis, MO) was dissolved in 10 mM phosphate buffer, equilibrated under 1 atm of carbon monoxide in a sealed glass tonometer, and then reduced with sodium dithionite. The purity of the preparation was checked by isoelectric focusing. The fluorescence spectrum of a MbCO sample from the preparation was recorded to ensure that no chromophore contaminant was present. For both Hb and Mb samples, typical sample concentrations ranged between 150 and 400 μM in heme.

The β-subunits were prepared by the oxidation of sulfhydryl groups that stabilize the hemoglobin tetramer using *p*-mercuriobenzoate (Bucci & Fronticelli, 1965). The free sulfhydryl groups were rereduced using 3 mM dithiothreitol. The β-subunits were further purified twice on a DEAE-Sephadex column. The purity of the β-product was estimated by isoelectric focusing. After extensive dialysis against a 10 mM phosphate buffer (pH 7) and vacuum concentration, the free β-chains were stored under 1 atm of carbon monoxide in liquid nitrogen until use. Under these conditions, no degradation of the isolated subunits was observed during storage. The solutions of free β-subunits are referred to as β_4 solutions at the concentrations used in the present experiments (400 μM in heme).

Measurement of TRRR Spectra

The time-dependent resonance Raman signal was observed using an experimental apparatus similar in many respects to that used previously (Petrich et al., 1987), however, with improvements in the laser system that permit longer signal averaging.[1] In the present experiments, the Raman beam at 435 nm, which is in resonance with the Soret band of all species observed, was generated by using the frequency-doubled output of a chain of three amplifiers using laser dye LDS867. The frequency bandwidth of the Raman beam was fixed using a bandpass filter with a 6 Å bandwidth after a cuvette containing H_2O was used to generate a continuum. The LDS867 amplifiers were pumped by the output of a frequency-doubled injection-seeded YAG laser at 30 Hz and functioned in a regime saturated in the femtosecond pulse (Migus et al., 1980). This apparatus leads to a consistently stable 435 nm beam over nearly an order of magnitude change in the intensity of the input pulse from the continuum and permits signal averaging for many hours with little drift. After frequency doubling to 435 nm, the bandwidth of the Raman probe pulse was 25 cm^{-1}, and the pulse duration was 700 fs. Typical Raman probe pulse energies were 500 nJ/pulse.

At the energies obtainable at 435 nm in the present apparatus, there was no detectable photodissociation of HbCO by the probe pulse alone. The probe beam was cylindrically focused with dimensions of 100 × 400 μm at the sample. No power broadening effects were observed under the conditions of the experiment. However, given the 35 cm^{-1} spectral bandwidth of the convolution of the probe pulse with heme Raman bands, it is difficult to rule out contributions to line broadening on the order of 5 cm^{-1} or

[1] Previous TRRR experiments (Petrich et al., 1987) used a YAG laser with a 10 Hz repetition rate and two stages of LDS867 amplification. The frequency-doubled amplified pulses were further amplified in a coumarin dye amplifier. The lower repetition rate and inherent long-term instability of pumping a laser dye at 355 nm limited the signal averaging times in earlier work (Petrich et al., 1987).

less. The data obtained in the experiments described in this paper are measurements of the relative intensity and frequency changes in Raman bands as a function of time. Raman difference spectra were obtained by subtracting an acquisition with a negative time delay (probe arrives before pump) from an acquisition at a positive time delay (probe arrives after pump). Equilibrium spectra were obtained either by allowing the Raman probe pulse to arrive at the sample 5 ps before the pump or as one-color experiments using 435 nm pulses. The difference spectrum at equilibrium (HbCO subtracted from deoxy-Hb) is then compared to several time-delayed Raman difference spectra of photolyzed Hb*(CO).

The pump pulse used in these experiments was a 100 fs pulse centered at 570 nm with an energy of 50 μJ/pulse. The pulses were made collinear using a dichroic mirror that had high reflectivity at 570 nm at an angle of 45 ° and high transmissivity at 435 nm. Experiments were done in which the pump intensity was reduced by one-half and one-quarter, and the signal size decreased proportionally with no detectable change in form.[2] The extent of photolysis (ca. 50%) indicates that the pump pulse intensities are about twice those used extensively in femtosecond transient absorption measurements. The timing between pump and Raman scattering pulses was determined using a parallel transient absorption experiment in which the photolysis of a sample of HbCO or deoxy-Hb was monitored. The transient absorption spectra were recorded using a single diode with no reference beam and no correction for pump intensity fluctuations. Transient absorption experiments were performed before and after each TRRR experiment.

The Raman-scattered light was collected by a camera objective and focused onto the slit of a 1 m monochromator (Jobin-Yvon). Typical slit widths used were 400−500 μm. The resolution was limited by the spectral bandwidth of the 435 nm pulses used to probe the sample. In the low-frequency region, a 1000 cm^{-1} bandpass filter with a very sharp cutoff below 437.6 nm was used as a Rayleigh filter. In addition, a 2 mm BG-25 filter was used to eliminate stray light due to the interaction of the pump pulse with the sample from entering the monochromator.

Ammonium sulfate (1 M $(NH_4)_2SO_4$) was used as an internal standard in some of the samples. There is a large Raman band for $(NH_4)_2SO_4$ at 983 cm^{-1}. The width of the window along the spectral axis of the microchannel plate detector was approximately 500 cm^{-1}, and thus it was convenient to calibrate the relative intensity of either of the known RR peaks at 679 (ν_7) and 1355 cm^{-1} (ν_4) in deoxy-Hb (and corresponding peaks in ligated species) against the internal standard.

RESULTS

The TRRR signals observed in deoxy-Hb and deoxy-Mb are discussed in order to determine the contribution from heme photophysics to the TRRR signal in a species where the heme is photoexcited, but no chemical change occurs. Subsequently, the TRRR data from photolyzed Hb*(CO), β_4*(CO), and Mb*(CO) will be examined for both the photophysical and conformational changes apparent in the signal. Appropriate comparisons will be made in order to separate the photophysical contribution from the conformational contribution to the resonance Raman signal.

The data obtained at times subsequent to the excitation flash are presented as Raman difference spectra. The difference is between two identical two-color experiments that differ only in that one has the delay set so that the Raman pulse arrives before the excitation pulse (-5 ps), while in the second experiment the Raman pulse arrives at a positive delay time (i.e., after the excitation pulse). The Raman spectrum at −5 ps is identical to the equilibrium Raman spectrum obtained using only the probe beam at 435 nm (one-color spectrum).

All kinetic traces of transient absorption (ΔA) shown in the figures were obtained using a parallel transient absorption experiment in which the pump and probe beams used in the Raman experiment were diverted into an absorbance cuvette with an optical path length identical to that of the Raman cuvette.

TRRR Spectra of Deoxy-Hb and Deoxy-Mb

Intensity Changes in the Raman Difference Spectra. The resonance Raman spectra of deoxy-Hb at four different delay times before and after a photolysis flash are shown in Figure 1. All of the major peaks in the deoxy-Hb RR spectrum reported elsewhere are found in the observed RR signal in Figure 1A obtained at a probe delay time of −5 ps (Bangcharoenpaurpong et al., 1984). The peak marked with an asterisk, at 983 cm^{-1}, is an internal standard (1 M $(NH_4)_2SO_4$). The peak at 212 cm^{-1} is the ν_{Fe-His} out-of-plane mode (Kitagawa et al., 1979). The in-plane A_{1g} modes observed are ν_4 at 1355 cm^{-1}, ν_7 at 679 cm^{-1}, and possibly ν_8 at 344 cm^{-1}. An in-plane B_{1g} mode observed is ν_{16} at 766 cm^{-1}. The core size marker region from 1450 to 1650 cm^{-1} is spectrally congested; however, the modes that appear are probably a combination of ν_2 and ν_{37} at $\approx$ 1574 cm^{-1} and the vinyl stretching frequency at $\approx$ 1624 cm^{-1}.

Raman difference spectra obtained at three times (1, 2, and 10 ps) subsequent to the photolysis flash are shown in Figure 1B−D. Baseline subtractions were performed after the raw Raman difference spectrum had been obtained. Two low-frequency regions, 180−550 and 550−800 cm^{-1}, required the subtraction of cubic and linear baselines, respectively, to obtain the Raman difference spectra shown in Figure 1B−D. In the high-frequency region, 1100-1700 cm^{-1}, the form of the baseline was nearly linear. There is a clear reduction in the intensity and frequency shift of the electron density marker mode, ν_4, at 1355 cm^{-1}. The intensities of the ν_7 mode at 679 cm^{-1} and the low-frequency modes are reduced as well. All changes are largest at 1 ps and decrease to zero by 10 ps.

The modes that showed no frequency shift for all time points obtained were globally fit to a Lorentzian model given by

$$L(\omega) = A_0 \frac{\Gamma}{\pi[\Gamma^2 + (\omega - \omega_0)^2]} \qquad (1)$$

where Γ is the Lorentzian full width at half-maximum (fwhm), ω_0 is the center frequency, and A_0 is the amplitude. Since any given mode was constrained to have the same

[2] At 50% photolysis the photoexcited sample is in a saturated regime. The deviation from linearity at $\Phi = 0.50$ relative to $\Phi = 0.25$ is 20% due to saturation. Given the error inherent in the smaller signal at low pump intensity, our observation is that we are in the expected regime of saturation and there are no additional nonlinear effects.

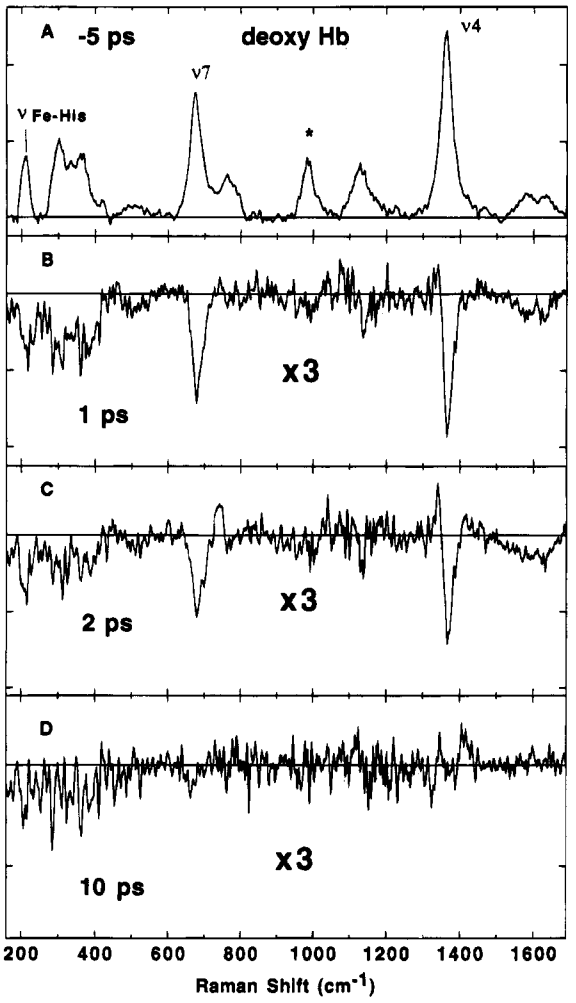

FIGURE 1: Time-resolved resonance Raman spectra of deoxyhemoglobin. Resonance Raman excitation was at 435 nm and photoexcition was at 570 nm. (A) Spectrum at −5 ps represents the equilibrium deoxy-Hb resonance Raman spectrum. The Raman bands ν_{Fe-His}, ν_7, and ν_4 are labeled. The internal standard sulfate peak is marked with an asterisk. (B) Spectrum at 1 ps delay. (C) Spectrum at 2 ps delay. (D) Spectrum at 10 ps delay. All positive delay times are magnified by a factor of 3 with respect to the equilibrium spectrum in part A.

fwhm Γ and ω_0 at all time points, the amplitude A_0 is directly proportional to the relative scattering intensity of the mode as a function of time. The quality of the fits at various delay times did not depend on the value of Γ within the error limits of ± 4 cm^{-1}. This justifies the use of a single value for Γ for the purpose of fitting the Raman difference spectra.

The intensity changes were monitored by calibrating both the 1355 and 6479 cm^{-1} Raman bands to an absolute internal standard of 1 M $(NH_4)_2SO_4$ [rms (root mean square) errors of ±5%]. This could be accomplished on a single spectral window of the multichannel plate detector. These two Raman bands then served as relative intensity standards ($I_{standard}$) for Raman bands less than 600 cm^{-1} and greater than 1400 cm^{-1}. The relative intensity of a mode at a given delay time, I_r ($=I_{mode}/I_{equilibrium}$), of a Raman band was calculated from the experimentally measured intensity relative to the sulfate absolute standard, I_{mr} ($=I_{mode}/I_{standard}$), using the formula

$$I_r = (I_{mr} - 1 + \Phi)/\Phi \qquad (2)$$

where the photolysis yield Φ was obtained from the relative

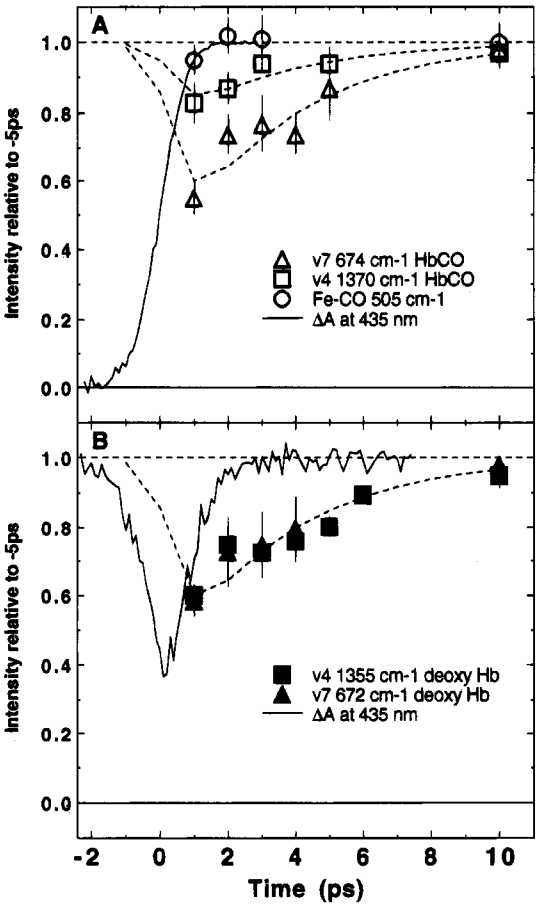

FIGURE 2: Time dependence of the Raman scattering intensity of HbCO and deoxy-Hb compared to an internal standard of 1 M $(NH_4)_2SO_4$. (A) The relative intensities of the ν_4, ν_7, and ν_{Fe-CO} Raman modes of HbCO are shown (open symbols) along with 3.5 ps decay functions convolved with the probe pulse (dashed lines). The intensity is measured relative to the intensity at −5 ps and then normalized to the difference in scattering cross section between HbCO and deoxy-Hb measured using an internal standard to calibrate the intensity of the ν_7 mode. The solid line is ΔA at 435 nm for HbCO obtained in a parallel transient absorption experiment. (B) The relative intensities of the ν_4 and ν_7 modes of deoxy-Hb are shown (solid symbols) normalized to the intensity at −5 ps. The dashed line is the same decay function used for the ν_7 mode in part A. The solid line is ΔA at 435 nm for deoxy-Hb obtained in a parallel transient absorption experiment.

intensity of the normalized Fe−CO stretching mode at 505 cm^{-1} (see below). Equation 2 was applied to each time delay separately to obtain the time dependence of the Raman intensities.

The time dependence of the intensity reduction of the two largest modes in the Raman spectrum of deoxy-Hb is shown in Figure 2B. The 1 ps point appears to have an anomalously low intensity compared to the others. This can be explained by the trivial mechanism that the extinction coefficient is lower for the rapid phase of heme excited-state relaxation ($\tau \approx 300$ fs), called Hb_I* (Martin et al., 1983b; Petrich et al., 1988), as seen in ΔA of the transient absorption trace in Figure 2B. The relaxation time of the intensity changes is approximately 3.5 ps, which is significantly longer than Hb_I*. There is a slower phase of relaxation ($\tau \approx 3.2$ ps) in deoxy-Hb, due to an excited state, Hb_{II}*, that is not observed in ΔA at 435 nm because this wavelength is nearly an isosbestic point for the slower phase (Petrich et al., 1988). The observed intensity changes have been normalized to an internal standard, which corrects for any change in the

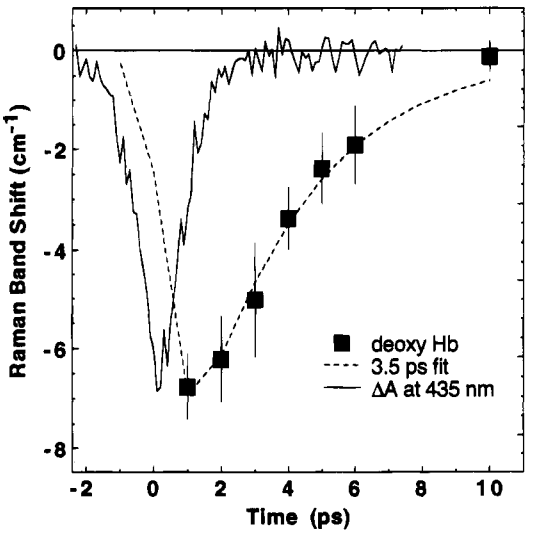

FIGURE 3: Time dependence of the frequency shift of the ν_4 mode of deoxy-Hb. The kinetic trace in the figure (solid line) is ΔA at 435 nm for deoxy-Hb obtained with the same pump−probe arrangement used for the Raman experiment.

internal absorbance of the sample due to an inner filter effect at the Raman-shifted wavelength on the time scale of the 3.5 ps relaxation process. The ν_7 mode was used to estimate changes in the relative intensity of modes in the low-frequency region where no internal standard Raman bands were available. The modes at 212, 304, 370, and 1124 cm^{-1} show the same intensity dependence as ν_7 (rms errors of ±10%). The relative intensity changes of the modes in the core size marker region could not be analyzed reliably due to spectral congestion. We conclude that the changes in the resonance Raman intensity of the ν_4, ν_7, and low-frequency modes are due to heme photophysics (Franzen et al., 1994a).

The same extent of photolysis, or Φ, was assumed in samples of deoxy-Hb and HbCO (or Mb and MbCO) of identical concentrations. The absorbance at the pump wavelength (570 nm) was ca. 1.2 times as great in HbCO as in deoxy-Hb, leading to a possible systematic difference in photolysis yield between the two species. In order to estimate the error inherent in the determination of the extent of photolysis, the fits of relative intensity and frequency were also done using the limiting error values of the photolysis measurement. The maximum possible systematic error in assuming the same photolysis yields for both HbCO and deoxy-Hb could lead to relative intensities of at most 0.1 lower in Figure 2B for deoxy-Hb (i.e., if $\Phi \approx 0.4$ instead of 0.5 measured for HbCO). The systematic error may be smaller than this due to the fact that the volume of scattering hemes in deoxy-Hb is smaller than that in HbCO, because the absorbance ratio at the Raman excitation wavelength (435 nm) is ϵ(deoxy)/ϵ(CO) ≈ 1.8. Adjustment of the wavelength at 570 nm so that it is identical in both HbCO and deoxy-Hb would have the disadvantage of increasing the disparity in internal absorbances at the scattering wavelength.

Data were obtained under similar conditions for deoxy-Mb samples without an internal standard. For both the ν_4 and ν_7 modes, sufficiently stable laser conditions allowed the observation of the relative intensity without normalization of the peak intensities to that of an internal standard. This procedure is justified by the absence of large systematic changes in the intensity of the internal standard observed in Hb samples. In deoxy-Mb, results similar to those shown in Figure 2B were obtained for both the ν_4 and ν_7 modes (data not shown).

Table 1: Frequency Shift of the ν_4 Raman Band in Photolyzed Hb* and Mb* and in Photoexcited Deoxy-Hb and Deoxy-Mb

time (ps)	shift (cm^{-1})[a]					
	Hb*(CO)	Mb*(CO)	Δ_{CO}[b]	deoxy-Hb	deoxy-Mb	Δ_{deoxy}[b]
1.0	−6.2 (0.6)	−2.9 (0.8)	−3.3	−6.8 (0.6)	−4.5 (1.8)[d]	−2.3
2.0	−6.3 (0.2)	−4.2 (0.6)	−2.1	−6.2 (0.8)	−6.0 (1.6)[d]	−0.2
3.0	−5.5 (0.4)	−3.2 (0.7)	−2.1	−5.0 (1.2)	−4.8 (1.4)[d]	−0.2
4.0		−3.2 (0.8)	−1.8[c]	−3.4 (0.9)	−2.2 (1.5)[e]	−1.2
5.0	−4.4 (0.4)		−1.5[c]	−2.4 (0.7)	−3.3 (1.5)[e]	0.9
6.0		−2.4 (0.7)		−1.9 (0.6)		
10.0	−3.1 (0.5)	−0.7 (0.7)	−2.4	−0.1 (0.3)	−0.9 (1.5)[e]	0.8
60.0	−2.5 (0.4)	−0.4 (0.4)	−2.1	0.2 (0.5)	−0.9 (1.5)[e]	1.1

[a] In each case, Hb or Mb, the shift is given relative to the frequency of the deoxy-Hb or -Mb band, respectively, at equilibrium. [b] The difference frequencies are calculated as $\Delta_{CO} = \nu$(Hb*) − ν(Mb*) and $\Delta_{deoxy} = \nu$(deoxy-Hb) − ν(deoxy-Mb). [c] Values are based on an extrapolation of data using the available time points. [d] The larger rms errors in the deoxy-Mb data reflect the fact that this measurement was made on only two separate samples. [e] Measurements were made on only one sample, and thus errors are a lower bound estimate.

Similar decreases in the picosecond time-resolved Stokes−Raman spectrum were observed using 8 ps pulses with excitation in the N band at 355 nm (Lingle et al., 1991). The decreases in intensity are similar in that they were relatively uniform across the Raman spectrum and the estimated decay time obtained from deconvolution was 2−5 ps, bracketing our observed decay time. Experiments using saturation Raman spectroscopy also show a reduction in the intensity of the Raman signal due to a bottleneck state with a 2.0 ± 0.7 ps lifetime (Li et al., 1992). In those experiments, the intensity dependence of the Raman signal for deoxy-Mb obtained using 10 ns pulses is used to extract Stokes and anti-Stokes excited-state Raman spectra, which have smaller cross sections than the ground-state spectra and shifted ν_4 bands similar to that described in the next section.

Frequency Shifts of the Electron Density Marker Band. In order to describe the frequency changes quantitatively, a shifted Lorentzian model was employed:

$$L_S(\omega) = A_0\left[\frac{A_S\Phi\Gamma}{\pi[\Gamma^2 + (\omega - \omega_0 - \omega_S)^2]} + \frac{(1-\Phi)\Gamma}{\pi[\Gamma^2 + (\omega - \omega_0)^2]}\right] \quad (3)$$

where ω_S is the magnitude of the shift in the center frequency and A_S is an asymmetry parameter that is proportional to the relative intensity of the mode in the photoproduct. The amplitude A_0, center frequency ω_0, and fwhm Γ were simultaneously fit to all of the time delays, allowing the relative intensity A_S and frequency shift ω_S to be determined independently for each time delay. As shown in Figure 3 and Table 1, the maximum shift ω_S observed in the ν_4 Raman band is −6.8 ± 0.6 cm^{-1} at 1 ps and it decays to the ground-state value with a time constant of ≈3.5 ps. Based on this type of analysis, the frequency changes have a time dependence similar to that of the intensity changes described in the previous section. The frequency changes of the 1355 cm^{-1} Raman band shown in Figure 3 are significant over the same time range as the intensity changes.

The other observed modes were also fit to a shifted Lorentzian model in which the relative amplitude and

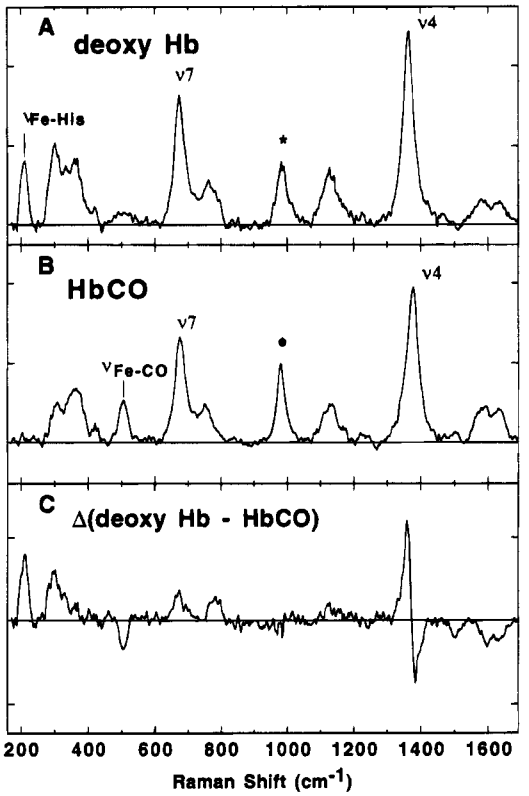

FIGURE 4: (A) Raman spectrum of HbCO at equilibrium. (B) Raman spectrum of deoxy-Hb at equilibrium. (C) Raman difference spectrum Δ(deoxy-Hb − HbCO) at equilibrium on the same scale as the spectra in parts A and B. In both (A) and (B), Raman scattering intensities were obtained using 435 nm Raman excitation in a two-color experiment in which the Raman pulse arrives at the sample 5 ps prior to the 570 nm pump pulse.

frequency of the RR band at time points after the excitation flash were adjustable parameters. There is a small but detectable shift in the region of the ν_7 and ν_{16} modes.

The frequency changes in TRRR of deoxy-Mb were found to be similar to those in deoxy-Hb as shown in Table 1. It was found that a $\approx$2 cm^{-1} larger negative shift in the ν_4 band for the early time delays (τ < 5 ps) was obtained if $\Phi \approx 0.4$ (instead of $\Phi \approx 0.5$ used in the fits listed in Table 1). Likewise, values of $\approx$1 cm^{-1} smaller negative shift were obtained if $\Phi \approx 0.6$ (τ < 5 ps). Band shifts of ≈ -9 cm^{-1} for ν_4 have been reported in the saturation Raman spectra of deoxy-Mb (Li et al., 1992). The ν_4 bandshift is the only major bandshift observed in the TRRR spectrum, in agreement with the saturation Raman experiments of Li et al. (1992).

TRRR Spectra of Photolyzed Hb(CO), Mb(CO), and β_4*(CO)*

Comparison of Equilibrium Deoxy-Hb and HbCO Raman Spectra. In order to compare the time-dependent changes in HbCO to those in deoxy-Hb, the difference in the equilibrium Raman spectra of HbCO and deoxy-Hb is used as a reference point. The HbCO equilibrium RR spectrum is shown in Figure 4B. The HbCO modes include many of the same modes observed in deoxy-Hb (Figure 4A), with the addition of the iron−ligand mode ν_{Fe-CO} at 505 cm^{-1} (Armstrong et al., 1982; Tsubaki et al., 1982), a shift of the electron density marker (ν_4) mode to 1370 cm^{-1}, and the modes ν_3 at 1494 cm^{-1} and a combination of ν_2 and ν_{37} at $\approx$1578 cm^{-1} in the core size marker region. A deoxy-Hb − HbCO difference spectrum is shown in Figure 4C. There are several characteristic differences between deoxy-Hb shown in Figure 4A and HbCO shown in Figure 4B. First, in the low-frequency region, two unique deoxy-Hb modes appear at 212 and 304 cm^{-1}. The Fe−CO stretch at 505 cm^{-1} is absent from deoxy-Hb, giving rise to the intensity reduction at 505 cm^{-1} in the equilibrium Raman difference spectrum. There is an increase in the shift scattering intensity of the modes at 679 and 766 cm^{-1}. There are a large shift and an increase in the intensity of the electron density marker mode at 1370−1355 cm^{-1} in the Raman difference spectrum. At frequencies higher than 1400 cm^{-1} there are an intensity reduction and a shift of several bands in the core size marker modes, indicating that the iron is no longer in the heme plane in deoxy-Hb. This same information is contained in the appearance of the Fe−His out-of-plane mode at 212 cm^{-1}, which is resonantly enhanced for a domed heme iron configuration (Kitagawa et al., 1979). There is an overall increase in the deoxyHb scattering intensity by a factor of 1.4 ± 0.15 relative to HbCO, which is likely due to the relative extinction coefficient at 435 nm of deoxy-Hb compared to HbCO.

The time-dependent changes in photolyzed HbCO contain the evolution of these changes over a range of time scales, including those due to photophysics already discussed for deoxy-Hb and changes in the signal due to changes in conformation, which are sensed by the electronic structure of the heme. The equilibrium HbCO RR spectrum is shown in Figures 5 alone with the Raman difference spectra obtained at three different time delays subsequent to the photolysis flash (1, 2, and 10 ps). The changes observed in this case are more complicated than those observed earlier for deoxy-Hb and require a detailed examination of both the electron density marker mode and the Fe−His out-of-plane mode in order to determine the information available on conformational changes.

Intensity Changes in the Raman Difference Spectra. During the first few picoseconds following the photolysis flash, there is an overall transient reduction in the intensity of the RR bands at 225, 304, 679, 766, 1124, and 1355 cm^{-1} and in the core size marker region (1450−1650 cm^{-1}) relative to their ultimate magnitude in the equilibrium deoxy-Hb − HbCO difference spectrum shown in Figure 4C. The transient intensity changes of three modes relative to their values in the equilibrium deoxy spectrum are shown in Figure 2A. Similar changes in the relative intensity were also observed in photolyzed MbCO (data not shown). The relative intensity of the ν_7 mode is very similar to the transient intensity changes that were observed in deoxy-Hb and -Mb (vide supra). As seen in Figure 2A, the ν_4 mode shows a systematically larger relative intensity, but it decays with the same time constant as the ν_7 mode. The mode at 1124 cm^{-1} shows behavior similar to that of the ν_4 mode (data not shown), while the remaining low-frequency modes at 225, 304, and 370 cm^{-1} show a 10% (or less) relative intensity reduction compared to the ν_7 mode during the first few picoseconds (data not shown), with larger rms errors of ±10%. Note that similar reductions were observed in deoxy-Hb. The intensity reduction and shift of the modes in the core size marker region occur instantaneously (less than 1 ps). Likewise, the mode at 1494 cm^{-1} bleaches as observed in the equilibrium spectrum for the photolyzed species. Note

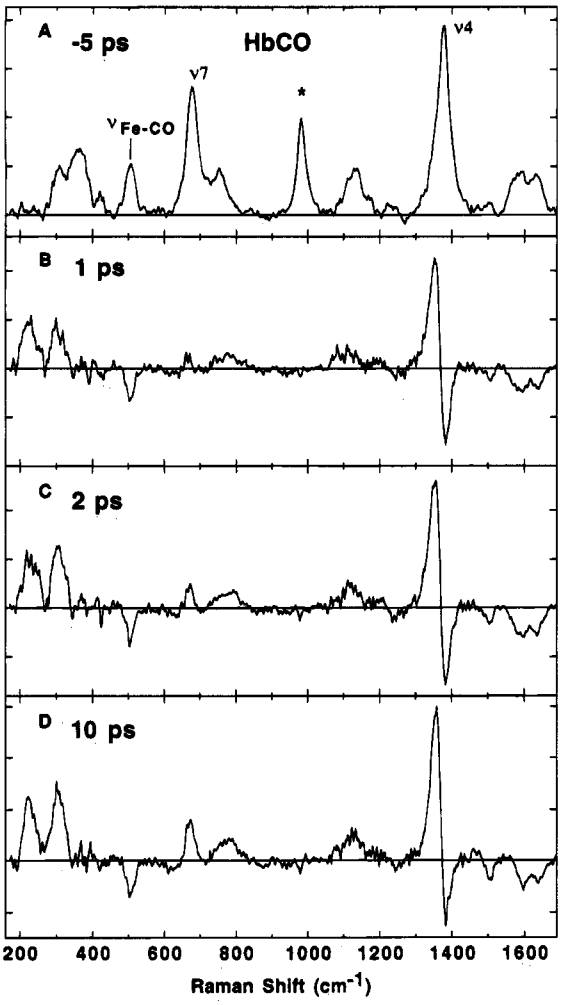

FIGURE 5: Time-resolved resonance Raman spectra of hemoglobin–CO. Resonance Raman excitation was at 435 nm and photoexcition was at 570 nm. (A) The spectrum at −5 ps represents the equilibrium deoxy-Hb resonance Raman spectrum. The Raman bands ν_{Fe-His}, ν_7, and ν_4 are labeled. The internal standard sulfate peak is marked with an asterisk. (B) Spectrum at 1 ps delay. (C) Spectrum at 2 ps delay. (D) Spectrum at 10 ps delay. All delay times are plotted on the same scale as the equilibrium spectrum in part A.

that the increasing asymmetry in the Raman difference signal of the electron density marker band ν_4 seen in Figure 5 is due to the fact that the intensity of the ν_4 band in the deoxy-Hb photoproduct is ≈1.4 times as large as in HbCO. There is no significant difference in the Raman spectra between 10 and 60 ps (or any subsequent time measured up to 300 ps).

The Fe−CO stretching mode at 505 cm^{-1} shows no change in intensity at any time after the photolysis flash (relative to long time values of greater than 60 ps). This is expected since the observed intensity of ν_{Fe-CO} is due to the population of hemes that was not photoexcited, and this population should not change in the absence of ligand recombination. Except for a small reduction in intensity at the 1 ps time delay, there is no evidence in these data of a fast geminate process in which 15% of the photodissociated CO recombines with a time constant similar to that of the state Hb_{II}* (τ = 3.2 ps) given the error of ±4% in the intensity of ν_{Fe-CO} (Petrich et al., 1988), in agreement with picosecond time-resolved infrared data (Anfinrud et al., 1989). Otherwise, the most rapid phase (ca. 50%) of CO geminate recombination has a lifetime of ≈50 ns in hemoglobin (Hofrichter et al., 1983). The intensity of ν_{Fe-CO} in Hb* relative to that in HbCO was used to calibrate the extent of photolysis in the sample. For most of the experiments reported here, Φ = 0.53 ± 0.04.

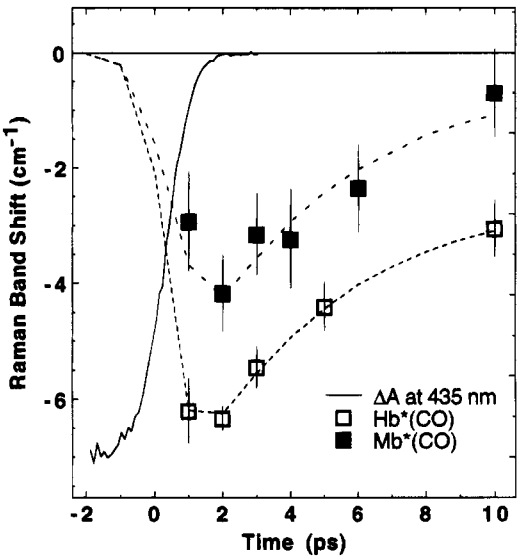

FIGURE 6: Time dependence of the frequency of the ν_4 mode of HbCO (open squares) and MbCO (solid squares). The kinetic trace in the figure (solid line) is ΔA at 435 nm for HbCO obtained with the same pump–probe arrangement used for the Raman experiment.

At the incident frequency it is clear that ΔA at 435 nm increases rapidly after photolysis and remains constant on the picosecond time scale (less than 1% change out to 300 ps). As was observed in deoxy-Hb, the presence of a transient due to Hb_{II}* (τ = 3.2 ps) does not appear in the transient ΔA at 435 nm, since 435 nm is an isosbestic point of the transient spectrum of Hb_{II}* (Franzen et al., 1994a).

Frequency Shifts of the Electron Density Marker Band. In HbCO, as in deoxy-Hb, there is a time-dependent frequency shift of the electron density marker or ν_4 band on a time scale of less than 10 ps. However, as shown in Figure 6, this band does not relax to the equilibrium deoxy value, but rather to a shifted value that is 2−3 cm^{-1} lower in energy than the equilibrium value. This observation is consistent with previous work on the TRRR of this Raman band using one-color experiments with 25 ps and 10 ns pulses. In addition, the values presented here are qualitatively consistent with the data obtained in a previous two-color resonance Raman experiment (Petrich et al., 1987). In previous work, there was no possibility of independently determining the extent of photolysis since only high-frequency data were obtained. If the value given earlier of $\Phi \approx 0.5$ were used instead of the 0.4 value assumed by Petrich et al. (1987), the data presented in Table 1 of Petrich et al. (1987) would give nearly the same values as those shown in Figure 7 (cf. the discussion of bandshifts as a function of Φ earlier).

We wish to distinguish the bandshifts due to photophysics (Petrich, 1987) from the ca. −2 cm^{-1} ν_4 bandshift due to heme conformational changes (Scott & Friedman, 1984). Since there is no apparent gap between the time scale of the relaxation of the ν_4 band due to heme photophysics (Figure 7) and the appearance of the bandshift due to the tertiary structure change, we consider two possibilities. The first possibility is that the magnitude of the bandshift in HbCO due to heme photophysics is identical to that observed in

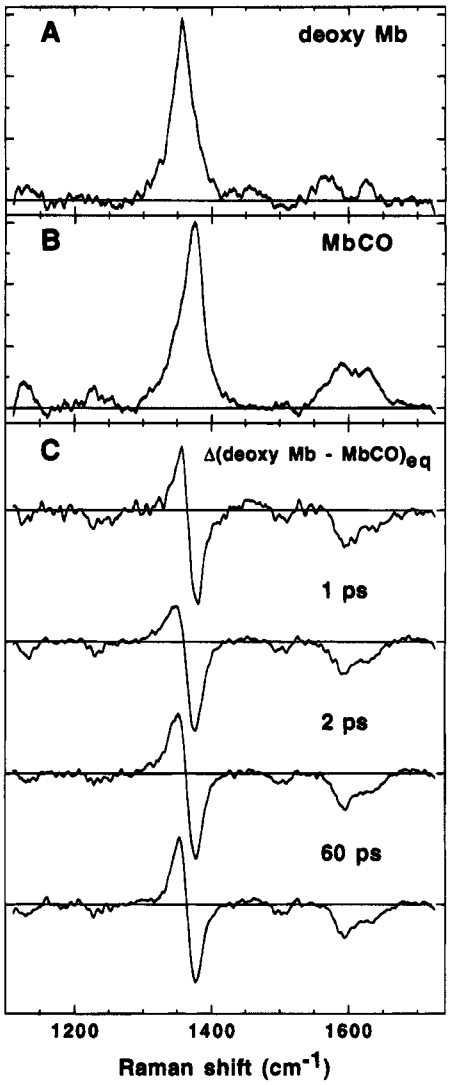

FIGURE 7: Time-resolved resonance Raman spectra of the high-frequency region of MbCO. (A) Spectrum at −5 ps is the equilibrium deoxy-Mb resonance Raman spectrum. (B) Spectrum at −5 ps is the equilibrium MbCO resonance Raman spectrum. The ν_4 band is slightly asymmetric in MbCO, but not in deoxy-Mb, HbCO, or deoxy-Hb. (C) Equilibrium difference spectrum Δ(deoxy-Mb − MbCO) and spectra at dealy times of 1, 2, and 60 ps.

deoxy-Hb, and thus the ν_4 bandshift due to conformational change arises on the same time scale as the decay of the signal due to heme photophysics (3−4 ps). The second possibility is that the ν_4 bandshift due to a conformational event occurs in less than 1 ps, and therefore the rapid phase of bandshift in HbCO attributed to heme photophysics is ≈2 cm^{-1} smaller than that observed in deoxy-Hb. In order to determine which of these possibilities holds, we have performed the same comparison on MbCO and deoxy-Mb. The data for the deoxy-Mb, MbCO, and photolyzed Mb*-(CO) species at three time delays (1, 2, and 10 ps) in the high-frequency region are shown in Figure 7. The comparison of the ν_4 bandshift shown as $\Delta_{CO} = \nu(Hb^*) - \nu(Mb^*)$ in column four of Table 1 reveals that the ν_4 bandshift due to heme photophysics is part of the signal only at the earliest times in photolyzed Hb*(CO), the rest being a constant offset of ca. −2 cm^{-1} due to a conformational change, as observed on longer time scales (Dasgupta et al., 1986; Friedman et al., 1982a).

Table 2: Position of the ν_{Fe-His} Mode in Different Species

	Hb	β_4	Mb
Eq deoxy	212	223	221[b]
1 ps	224	*a*	224[c]
60 ps	226	226	228[c]

[a] The 1 ps resonance Raman spectrum could not be obtained below 400 cm^{-1} in this sample due to a large feature associated with the Rayleigh line, which appeared at delay times of less than 3 ps. [b] In deoxy-Mb, Raman bands are observed at 221 and 240 cm^{-1}, comprising 75% and 25% of the total intensity, respectively (Argrade et al., 1984). These bands appear as a single broad band with our spectral resolution. The value given is the lower frequency band of a fit to two Gaussians, each with a fwhm of less than 35 cm^{-1}. [c] A Raman band is observed at ≈250 cm^{-1} in MbCO, which appears to be absent or much reduced in intensity in HbCO, in agreement with previous reports (Tsubaki et al., 1982; Wells et al., 1991). This mode is likely to be a pyrrole out-of-plane tilting mode (Choi & Spiro, 1983; Wells et al., 1991). Since this mode is absent from deoxy-Mb, the frequencies reported in the Mb* spectra were obtained by including this mode with fixed frequency and fwhm in a fit of the Raman difference spectra.

There are also small bandshifts in the region of ν_7 and ν_{16} and the core size marker region. These shifts occur on a sub-picosecond time scale and do not appear to change as a function of time. Both regions are spectrally congested, and we have not made any attempt to analyze them further. It should be noted, however, that the core size marker region changes in a manner that is qualitatively consistent with a domed heme iron and that the observation of this manifestation of heme doming has been observed previously on the sub-picosecond time scale (Petrich et al., 1987).

The Appearance of the Fe−His Out-of-Plane Mode. In the two-color experiment shown in Figure 5, the Fe−His resonance Raman band appears in Hb* at a +12 cm^{-1} shifted position (with respect to equilibrium deoxy-Hb) within 1 ps of the photolysis flash. The Fe−His out-of-plane mode appears in photolyzed Hb*(CO) at ca. 223 cm^{-1}, based on one-color time-dependent resonance Raman studies (Findsen et al., 1985b). This frequency is nearly the same as that observed in equlibrium deoxy-Mb as well as photolyzed Mb* (Findsen et al., 1985a). In deoxy-Hb (T state), the position of the Fe−His mode appears at 216 cm^{-1} in their work and 212 cm^{-1} in the spectra presented here. The intensity of the Fe−His out-of-plane mode in the equilibrium deoxy-Hb − HbCO Raman difference spectrum (Figure 4C) is smaller than that observed in the transient Raman spectrum (Figure 5B−D), in agreement with previous measurements (Bangcharoenpaurpong et al., 1984).

The low-frequency region in myoglobin is more complicated due to the presence of an additional low-frequency mode at 250 cm^{-1} in the MbCO, but not the deoxy-Mb, spectrum (Franzen et al., 1994c). Accurate determination of the frequency shift is obscured by these spectral changes (see Table 2). Therefore, we used β_4CO as a further test of the consistency of the observations in Mb*CO, Hb*CO, and previous experiments. The data for the low-frequency region of equilibrium and photolyzed β_4CO are compared in Figure 8. It is seen there that the position of the ν_{Fe-His} band in photolyzed β_4CO is the same as that in deoxy-β_4, both of which are in the R state. On the basis of these data, no significant differences between α- and β-subunits can be determined within the frequency resolution of a picosecond TRRR experiment. The results are summarized in Table 2, which shows a significant difference between deoxy-Hb in

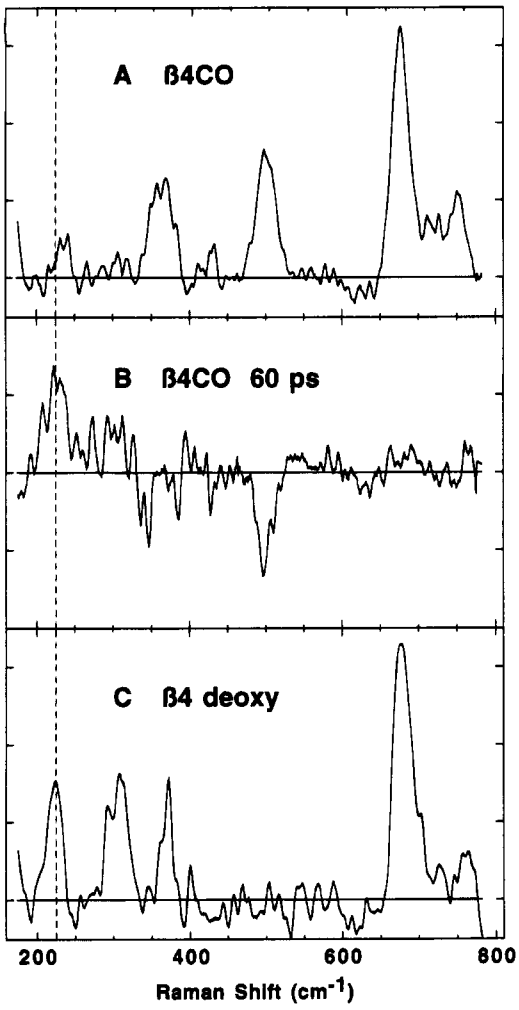

FIGURE 8: Comparison of the frequencies of the ν_{Fe-His} modes of β_4*(CO) and deoxy-β_4. (A) The low-frequency equilibrium β_4CO resonance Raman spectrum was obtained with a delay of −5 ps between the probe and pump beams. (B) The low-frequency Raman spectrum at 60 ps delay plotted on the same scale as part A. (C) The equilibrium deoxy-β_4 resonance Raman spectrum was obtained with a delay of −5 ps between the probe and pump beams. The dashed vertical line shows that the position of the ν_{Fe-His} mode in photolyzed β_4*(CO) appears in the same position as that of deoxy-β_4.

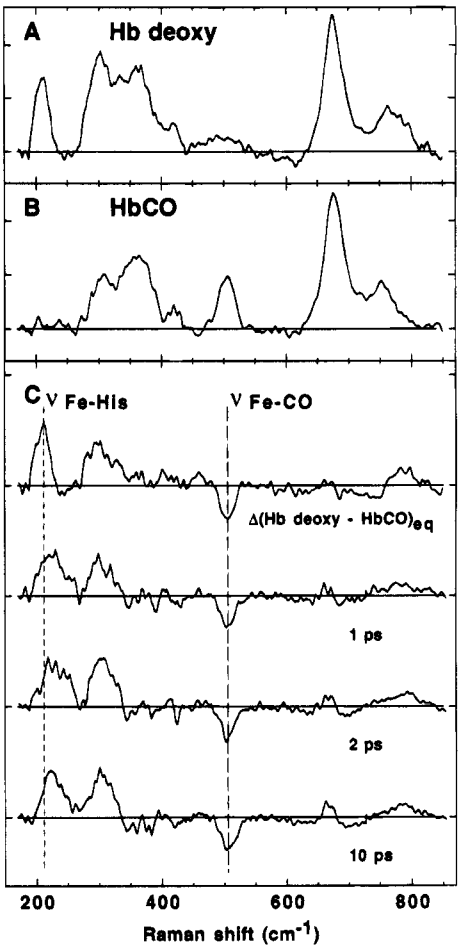

FIGURE 9: Time-resolved resonance Raman spectra of the low-frequency region of HbCO. (A) Spectrum at −5 ps is the equilibrium HbCO resonance Raman spectrum. (B) Spectrum at −5 ps represents the equilibrium deoxy-Hb resonance Raman spectrum. (C) Equilibrium difference spectrum Δ(deoxy-Hb − HbCO) and spectra at dealy times of 1, 2, and 10 ps. The spectra were normalized to the intensity of the ν_7 Raman band. By using the intensity changes of this hemoglobin Raman band as an internal standard, the effects of heme photophysics can be eliminated from the low-frequency spectrum (see text).

the T state and the remaining species, which all resemble the R state.

The data were fit to a model that includes changes in both intensity and frequency. No time dependence of the frequency shift for any of the low-frequency modes was found on the time scale from 1 to 200 ps. By 1 ps, the intensity of the ν_{Fe-His} mode is at least 90% (±10%) of the value at long times (60, 100, or 200 ps, depending on the data set). By the 10 ps time point, there is no reduction in intensity, suggesting that all phases of relaxation in the ν_{Fe-His} mode have time constants of 10 ps or less.

DISCUSSION

Separation of Photophysics from Conformational Changes

The Raman bandshifts and intensity changes described in the Results section can be ascribed to one (or more) of three possible phenomena: protein conformational changes, vibrational temperature, or excited electronic state. Time-dependent changes observed in deoxy-Hb and -Mb are assumed to be due to heme photophysics, exclusively. The similar, but smaller, time-dependent intensity reductions and ν_4 bandshift, which are observed to relax with a 3−4 ps time constant in Hb*(CO) and Mb*(CO), are assumed to have the same origin. The separation of photophysical signals from the signals due to conformational changes can be effected by assuming that the modes common to HbCO and deoxy-Hb (e.g., the ν_7 mode at 674 cm^{-1}) show intensity changes due to photophysics only, in both species. This being the case, it is possible to normalize the low-frequency region to this mode as a standard in order to determine whether the important modes that are indicative of heme doming (at 212 and 304 cm^{-1}) exhibit any time-dependent intensity dependence apart from heme photophysics. This normalization is shown in Figure 9, where it can be seen that there is little or no change in the intensity of the Fe−His out-of-plane mode after its appearance at 1 ps after the photolysis flash.

The time-dependent bandshift of Hb*(CO) in the ν_4 region can be separated into contributions from heme photophysics and conformational changes by observing the difference between a noninteracting monomer (photolyzed MbCO) and

a cooperatively interacting tetramer (photolyzed HbCO). These species both have a time-dependent shift in the ν_4 in common with their respective photoexcited deoxy species. The similar time course, but smaller magnitude of the ν_4 bandshift in the photolyzed, ligated species (compared to the photoexcited deoxy species) is described in Table 1. The origin of these photophysical processes in the respective species is discussed elsewhere (Franzen et al., 1994a). In the following section, we focus on the significance of the data relating to conformational changes in the structures of hemoglobin and myoglobin.

Correlation of the ν_4 and ν_{Fe-His} Bandshifts

The bandshift of the ν_4 mode has been studied extensively on a variety of time scales using one-color experiments (Dasgupta et al., 1986; van den Berg & El-Sayed, 1990; Scott & Friedman 1984). The ca. -2 cm^{-1} bandshift of ν_4 on the time scale of picoseconds to nanoseconds has been interpreted as being due to the nonequilibrium deoxyprotein structure. There are two phases of relaxation of the ν_4 bandshift, and the time scale of the final phase of relaxation of the shift is nearly the same as that of the quaternary structure change (Hofrichter et al., 1983). The relaxation of the shift in ν_{Fe-His} also occurs in two phases, although there is some question concerning the correlation of the relaxation rate of this mode with that of the ν_4 mode (Scott & Friedman, 1984). A linear relationship between the frequency shifts of these modes has been demonstrated for hemoglobins in different species and for myoglobin (Friedman et al., 1982a). It is therefore of interest to establish this correlation as part of the evidence for a domed heme on the sub-picosecond time scale. By comparing the ν_4 bandshifts of photolyzed HbCO and MbCO given in Table 1 and shown in Figure 7, it is evident that, at all positive delay times, there is a constant ν_4 bandshift of ca. -2 cm^{-1} in Hb* relative to deoxy-Hb as observed elsewhere. The observation of ν_{Fe-His} in a shifted position seen in Table 2 and Figure 9 establishes the correlation between the frequency shifts of ν_4 and ν_{Fe-His} on the subpicosecond time scale. These observations indicate that concerns about the interference of heme photophysics with the interpretation of TRRR studies based on the 10 ps (or longer) time scale are unwarranted (Asher & Murtaugh, 1983).

Origin of the Resonance Raman Intensity Enhancement and Frequency Shifts of ν_{Fe-His} and ν_4

The frequency shifts and resonance Raman intensity enhancement of the ν_{Fe-His} and ν_4 modes can be described qualitatively using a model in which it is assumed that resonance Raman enhancement is due entirely to a single excited electronic state (i.e., to *A*-term scattering resonant with the Soret absorption band). If we assume that enhancement of the Raman active modes is due to linear coupling (nuclear displacements in the excited state), the ν_4 in-plane mode should be sensitive to the population of the $e_g(\pi^*)$ orbital, which influences the bond strength (and hence bond length) of the bonds of the porphyrin macrocycle. For in-plane modes, the resonance Raman cross section is roughly proportional to the square of the nuclear displacement in the excited state due to the change in bond lengths (Myers & Mathies, 1987). For an out-of-plane mode the situation is more complicated. Vibronic coupling to other electronic states, such as metal-to-ligand charge transfer states (*B*-term scattering), may contribute (Bangcharoenpaurpong et al., 1984) along with the overlap of iron d orbitals of appropriate symmetry and symmetry lowering due to structural changes (Champion, 1988). In considering this latter possibility, the iron−histidine configuration as the iron moves out of the heme plane critically affects the mixing of iron d orbitals with the porphyrin π system. The configuration is defined by (1) the out-of-plane displacement following ligand photodissociation, a^* (defined relative to the average plane of the porphyrin ring), (2) the tilt angle of the iron−histidine bond, θ (relative to the heme normal), and (3) the azimuthal rotation, ϕ (about the heme normal). The origin of the resonance Raman intensity of the Fe−His vibrational mode results from the electronic overlap created by these symmetry-lowering factors. In the linear coupling model of resonance Raman intensities, the nuclear contribution to Soret enhancement of the ν_{Fe-His} out-of-plane mode can occur through the overlap of an iron d_{z^2} orbital with either occupied $a_{1u}(\pi)$, $a_{2u}(\pi)$, or virtual $e_g(\pi^*)$ orbitals (in the ground-state electronic configuration), which experience changes in population upon excitation. The Fe−Nϵ bond length changes (Nϵ is the proximal histidine nitrogen atom bonded to iron) in the excited state. The Nϵ lone pair orbital forms a σ-bonding interaction with the iron d_{z^2} orbital to form bonding (d_{z^2}+Nσ) and antibonding (d_{z^2}−Nσ) orbitals.

The intensity of the ν_{Fe-His} mode increases with increasing iron out-of-plane distance a^* due to the creation of overlap between the d_{z^2}−Nσ antibonding orbital and the $a_{2u}(\pi)$ porphyrin orbital (which is zero by symmetry for in-plane iron). The frequency of the ν_{Fe-His} mode is also affected by the out-of-plane distance since greater overlap of d_{z^2}−Nσ and $a_{2u}(\pi)$ leads to mixing, which increases the orbital population of the d_{z^2}−Nσ orbital (Champion, 1988). The frequency of ν_{Fe-His} depends on the iron spin state and increases dramatically for low-spin iron due to the change in bond order if the d_{z^2}−Nσ orbital is vacant (Saito & Kashiwagi, 1985). It has also been suggested that the ν_4 band frequency increases with increasing a^* due to the change in overlap of the d_{xz} and d_{yz} iron orbitals (of π symmetry) and the $e_g(\pi^*)$ antibonding orbital on the heme (Stavrov, 1993).

An increase in the tilt angle θ of the proximal histidine can give rise to mixing of the d_{z^2} orbital with the $e_g(\pi^*)$ orbital. The increase in orbital population of the $e_g(\pi^*)$ antibonding orbital in the ground electronic state is capable of lowering the frequency of ν_4 and, at the same time, increasing the frequency of ν_{Fe-His} (Friedman et al., 1990). This may explain the correlation between the Raman bandshifts of these two modes discussed in the preceding section and elsewhere (Friedman et al., 1982b).

The azimuthal angle ϕ contributes to resonance enhancement because, once tilted, the overlap of the d_{z^2}−Nσ antibonding orbital with both $a_{2u}(\pi)$ and $e_g(\pi^*)$ will be affected by this rotation angle (Bangcharoenpaurpong et al., 1984). A second origin of overlap due to ϕ involves His−N$\epsilon(\pi)$ orbitals with the iron d orbitals and a porphyrin of appropriate π symmetry (Friedman et al., 1990; Scheidt & Chipman, 1986).

We summarize by describing the configurational changes that appear best supported by experimental observations (Friedman et al., 1982b, 1990; Spiro, 1988). Iron out-of-plane displacement a^* increases the intensity of ν_{Fe-His}.

Changes in the azimuthal angle ϕ are important once a^* is sufficiently large for histidine rotations to occur with relatively less steric repulsion due to the porphyrin. The tilt angle θ is likely to be the major factor influencing the frequency shifts, as evidenced by the extensive correlations in R- and T-state hemoglobins from a variety of species (Friedman et al., 1990). In a specific model proposed by Friedman and co-workers, the frequency of ν_{Fe-His} is reduced by 6 cm^{-1} in the T state of deoxy-Hb due to the increase in θ. There is a hierarchy of dependence of the degrees of freedom available, since the angle of tilt θ is limited by F-helix displacements and heme−histidine repulsions (depending on the extent of a^*), and since the effect of ϕ depends on both a^* and θ.

Is Sub-picosecond Heme Doming Partial or Complete?

The normalized data in Figure 9 show that a very rapid rise in the intensity of the ν_{Fe-His} Raman band occurs on the same time scale as ligand photodissociation (within the 700 fs time resolution of the TRRR experiment). The intensity of the ν_{Fe-His} band is 90% of the maximal value (when normalized to the ν_7 mode in Figure 9) by 1 ps after photolysis and rises to the maximal value by, at most, 10 ps. Given rms errors in intensity of ±10%, and by assuming a linear relationship between the ν_{Fe-His} intensity and out-of-plane displacement a^*, the TRRR data suggest that $a^* = 0.40 \pm 0.05$ Å during the first picosecond in the case of Mb* (using deoxy−Mb $a_0 = 0.45$ Å as the equilibrium out-of-plane position in the ensuing discussion). This result agrees with the hypothesis that the transient absorption spectrum at 300 fs shows a domed heme iron (Martin et al., 1983b, 1984; Petrich et al., 1988) and the hypothesis that the heme iron out-of-plane vibration frequency is ca. 50 cm^{-1} (Zhu et al., 1994). The out-of-plane displacement time of 300 fs corresponds to one-half period of a heme iron vibrational cycle (Austin et al., 1989; Li & Zgierski, 1992), indicative of a critically damped motion of the heme iron.

The significance of heme doming in Hb*, which has a quaternary structure change, is different from that in Mb* or β_4* where only tertiary structural changes occur. In Hb, the heme iron is not completely relaxed until the deoxy-Hb (T state) configuration (Perutz, 1970; Baldwin & Chothia, 1979) is achieved after the quaternary transition on the microsecond time scale (Hofrichter et al., 1983). The similarity of the TRRR data for Hb*, Mb*, and β_4* suggests that tertiary relaxations in Hb* are similar to those in Mb* or β_4* and that the iron out-of-plane position, a^*, for these photolyzed species arrives at the *tertiary* equilibrium deoxy position, a_0, on the picosecond time scale. An additional set of quaternary configurational changes occurs in Hb, where the subunits interact strongly following the R → T transition on a longer time scale,[3] due to the large body of experimental data obtained on monomer Mb*.

Using $a_0 = 0.45$ Å for deoxy-Mb (Kuriyan et al., 1986) as the benchmark for a fully domed heme, there are several lines of evidence that have been used to suggest that the heme iron in Mb has not reached the full value a_0 on the picosecond time scale at room temperature. First, picosecond experiments on the core size marker region suggest that some residual core relaxation is still required to achieve the deoxy configurational in Mb* on the nanosecond time scale (Dasgupta et al., 1985). Although rich in information, the core size marker region is spectrally congested, and the interpretation of small shifts is not definitive. In the present study, we see no evidence for significant changes in the core size marker region beyond the initial appearance of deoxy-like core size Raman bands due to the domed heme, which appear on a sub-picosecond time scale.

A second line of evidence used to suggest that the final 20% of heme iron out-of-plane displacement occurs over a range of time scales from tens of picoseconds to nanoseconds comes from picosecond transient absorption spectra of the bandshift of band III in Mb at ambient temperature (Jackson et al., 1994). The comparison of the trajectory of the band III shift and the MD simulations in Petrich et al. (1991) has been used (Jackson et al., 1994) to buttress the point of view that the heme iron moves 80% out of the plane on the sub-picosecond time scale (compare this to the 90% ± 10% we find on the basis of the TRRR Raman), and the interpretation of the four trajectories in Petrich et al. has been used as evidence that the remaining 20% of heme iron displacement occurs on the 100 ps time scale (as opposed to the less than 10 ps we find on the basis of the data in Figure 9 and from other experiments). Concerning the MD simulations, it must be kept in mind that there are both nonequilibrium relaxations toward the deoxy geometry and equilibrium fluctuations about the evolving protein and heme geometries in the relaxation. The large equilibrium fluctuations require an average of a large number of trajectories in order to determine the average position of an atom or group. Perhaps for this reason, there are contrasting MD simulations that indicate that complete heme doming occurs on a time scale of less than 10 ps, in agreement with the interpretation of the TRRR results in Figure 9 (Li et al., 1993; Schaad et al., 1993). Furthermore, if we compare the trajectory (one or four) given in Figure 2 of Petrich et al. (1991) to the TRRR data in Figure 9, we find that the average iron position at 0.5 ps is at an average distance of 0.34−0.36 Å (out of 0.41 Å), or 83−88% of the equilibrium out-of-plane displacement (again compared to 90% ± 10% from the TRRR data presented here). In Figure 2B, the displacement is 0.39 Å at 1 ps, 0.37 Å at 2 ps, and 0.375 Å at 3 ps, presenting flucuations in the course of a relaxation apparent from Figure 2 (Petrich et al., 1991). These values correspond to 95%, 90%, and 91% of the total 0.41 Å displacement. The final 5 ps of the 10 ps window given in Figure 2B shows the iron at an average position of 0.39−0.40 Å or 95−98% of the total displacement. The data in Figure 2C show equilibrium fluctuations by ca. 40 ps about the long time value of 0.41 Å (i.e., the last 2−5% of heme iron out-of-plane displacement occurs with a lifetime of ca. 15 ps). We reach the conclusion that the data presented in Petrich et al. (1991) support the TRRR data presented here, indicating ultrafast doming within both the signal-to-noise ratio of the experiment and the equilibrium fluctuations present in the MD simulations. The origin of the frequency shift of a charge transfer band such as band III can be found in small changes iron position and,

[3] The more limited data available for Hb add the additional factor of quaternary structure changes to comparisons made in Mb*. There are longer lived time-resolved bandshifts in band III data in Hb (Sassaroli & Rousseau, 1987; Dunn & Simon, 1991), slower relaxations of TRRR on the core size marker region (Stein et al., 1982; Dasgupta & Spiro, 1986), and an increase in the intensity of ν_{Fe-His} as the temperature is lowered (Ondrias et al., 1983). These observations are comparisons of Hb* in the R state to deoxy-Hb in the T state.

more importantly, in the relaxations of dipolar and polarizable amino acid residues predominantly on the distal side. We have recently shown parallel behavior between the relaxations of the Soret band and band III in viscous medium between 250 and 290 K (S. Franzen and S. G. Boxer, manuscript in preparation). The relaxations of the Soret band are known to be correlated with distal residue relaxations and fluctuations on the basis of the work of Lambright et al. (1991). Thus, it appears that in the physiologically relevant temperature regime the distal side conformational changes occur on the nanosecond time scale, while iron out-of-plane motion occurs on the sub-picosecond to picosecond time scale. Since the rise in *intensity* of band III occurs on the sub-picosecond time scale (Jackson et al., 1994; Lim et al., 1993), this observable value may be an indicator of the nearly complete iron out-of-plane displacement we observe in the TRRR spectra of Hb*CO and Mb*CO on the sub-picosecond time scale.

The results obtained from a variety of studies at cryogenic temperature have been used to suggest that iron out-of-plane motion is hindered by protein conformations at these temperatures. We address the evidence for hindered iron motion and the bearing of these studies on the data we have obtained at physiologically relevant temperatures. A detailed model of kinetic hole burning (KHB), spectral (band III and Soret) bandshifts, spectral broadening mechanisms, and distributed CO rebinding kinetics exhibits a correlation (Srajer & Champion, 1991). However, the correlations between KHB and rebinding barriers, which have been substantiated (Srajer & Champion, 1991), do not uniquely determine the structural origin of these correlations. If all parameters were to depend on a single coordinate, e.g., a^*, it should be possible to deduce a simple correlation that explains all parameters. The influence of lowest energy barriers on a^* will be manifested at temperatures below 40 K, where greatly reduced ν_{Fe-His} intensities (<30% of room temperature) and increased frequencies ($\approx$8 cm^{-1}) are observed in Mb (Sassaroli et al., 1986; Ahmed et al., 1991). At $T < 5$ K, iron out-of-plane displacement is severely hindered and $a^* < a_0$ (Roder et al., 1984; Rousseau & Argade, 1986). At $T > 5$ K, magnetic susceptibility measurements have shown that the iron is high spin in Hb* (Roder et al., 1984) and significantly domed in Mb*, as determined by the frequency shifts of the core size marker modes, leading to the suggestion that $a^* \approx a_0$ (Rousseau & Argade, 1986). However, the question remains as to whether very small deviations from a_0 on the order of 0.1- or $0.2a_0$ may still play a significant role in determining the ligand rebinding dynamics and spectral shifts at these temperatures.

From 40 to 160 K, CO recombination occurs with measurable rates and KHB is observed (provided the sample is returned to <10 K to allow observation of the band III spectrum). The barriers that can be surmounted, leading to ligand rebinding (and KHB), are significantly lower than the barriers that lead to a relaxation in the frequency shift of band III (or the Soret band) in Mb*, which occurs to only limited extent below 160 K (Campbell et al., 1987; Steinbach et al., 1991; Srajer & Champion, 1991). By contrast, the intensity of the ν_{Fe-His} mode in Mb* (using 10 ns pulses) increases from 30% to 70% of the room temperature magnitude (Ahmed et al., 1991) as the temperature is increased from 40 to 160 K and continues to increase to 100% of the room temperature magnitude above 160 K (except for a small dip at 175 K near the glass transition temperature). Furthermore, the relaxation of the *frequency shift* in the ν_{Fe-His} band also occurs at generally higher temperatures than the relaxation of the *intensity* reduction. These observations are consistent with motions along a^* and ϕ, forming the lowest class of barriers, while the barrier to θ is higher, and distal side conformational changes have still higher barriers. The different dependencies of ν_{Fe-His} and band III as a function of temperature (Sassaroli et al., 1986; Ahmed et al., 1991; Nienhaus et al. 1992) and time at room temperature (Lim et al., 1993) suggest that the observable values may be correlated with other proximal side motions, such as the angle of tilt θ and azimuthal rotation ϕ of the proximal histidine, or distal side rearrangements accompanying ligand diffusion and approach to the deoxy structure, such as the distal His displacement by 1.4 Å in deoxy-Mb compared to MbCO (Kuriyan et al., 1986). Finally, we point out that even if the frozen configurations accessible in Mb* at low temperature are hindered due to protein conformational constraints, the thermal barriers may be easily crossed at room temperature, leading to a less hindered trajectory for a^* in Mb* at early times following ligand photolysis.

At room temperature, evidence obtained from picosecond time-resolved infrared (TRIR) spectroscopy (Causgrove & Dyer, 1993), picosecond phase grating spectroscopy (Richard et al., 1992), and picosecond TRRR (Findsen et al., 1985a) suggests that the major structural relaxations in Mb* are completed within 30 ps. Some aspects of the tertiary structural change may require $\approx$300 ps, as measured by time-resolved circular dichroism (TRCD) (Xie & Simon, 1991). TRCD is sensitive to more remote regions of the protein, since the conformation of several distant aromatic amino acid residues is the likely origin of the observed effect (Xie & Simon, 1991). The time-dependent relaxation of the Soret band in Mb* has been investigated as a function of solvent viscosity and single-site distal residue mutation by transient absorption spectroscopy on the nanosecond time scale at near-ambient temperature (Lambright et al., 1991; Ansari et al., 1992). These experiments demonstrate the sensitivity of changes in the transient absorption spectrum to protein relaxations, which have been demonstrated to correlate with the protein conformation in the distal pocket (Lambright et al., 1991; Tian et al., 1992). The evidence in Figure 9 suggests that these effects are not attributable to heme doming, which occurs on a 6 orders of magnitude shorter time scale. This view is further substantiated by the large viscosity dependence of Soret bandshift relaxation, band III shift relaxation, and recombination kinetics in Mb* and the absence of a viscosity dependence[4] of the ν_{Fe-His} intensity in a nanosecond TRRR experiment (Findsen et al., 1988). We conclude that the TRRR signal in Figure 9 is indicative of significant sub-picosecond heme doming at room temperature, $a^* > 0.9a_0$, giving a residual distance of at most 0.05 ± 0.05 Å by 1 ps after photolysis.

[4] The fact that the nanosecond TRRR experiments (Findsen et al., 1988) were done on Hb* does not weaken this argument. The changes in the nanosecond TRRR signal were consistent with complete subnanosecond out-of-plane motion (at the level of the tertiary structure change). However, there was an observed viscosity effect on the rate of quaternary structure changes.

Relationship between Ultrafast Conformational Changes and Cooperativity

The data presented here can be understood in the context of the theory of allostery advanced by Monod, with regard to the similarity of the properties of monomer subunits and the weakly interacting (R state) polymer form of the same protein (Monod et al., 1965). The ν_4 and ν_{Fe-His} bandshifts and intensity changes in the picosecond TRRR data are similar for photolyzed Hb*, Mb*, and β_4*, consistent with the hypothesis that a monomer subunit (Mb) will most closely resemble the properties of the weakly interacting cooperative protein (R-state Hb). The tertiary structural changes measured on the picosecond time scale are orders of magnitude faster than the transition R → T, which leads to strongly interacting subunits. The extent of the picosecond phase of tertiary F-helix motion is not definitively established by TRRR data that probe iron motion specifically; however, when compared to TRIR and other data, a picture emerges in which substantial tertiary relaxation has occurred on the same time scale we measure for heme doming. There is no a priori necessity for protein motion to occur on the picosecond time scale specifically; however, it is crucial that the potential energy available when the iron moves out of the heme plane be captured as rapidly as possible in localized motions of the protein, which can propel the subunits toward one another in an incipient phase of the quaternary structure change.

In the T state, both salt bridges and hydrophobic interactions responsible for the free energy of cooperativity may produce differences in Raman signals observed in the ν_{Fe-His} and ν_4 bands by means of the tension of the F-helix, which is transmitted to the iron−histidine complex. It is possible that the same interactions that reduce the ligand binding affinity in T-state Hb also change the resonance Raman intensity and frequency by increasing the tilt, and perhaps the out-of-plane distance of the iron, with respect to that observed in noninteracting photolyzed deoxy species such as Mb* and β_4*, even on the picosecond time scale. Thus, the positions of ν_4 and ν_{Fe-His} are the same for deoxy-Mb, deoxy-β_4, photolyzed Hb*, Mb*, and β_4* on the picosecond time scale, and it is only deoxy-Hb at equilibrium that shows a shift in these bands. These facts suggest that important parameters governing the conformation at the heme iron on a sub-picosecond time scale are similar for the weakly interacting and monomer globins and characteristically different from strongly interacting T-state globins.

CONCLUSION

The TRRR data presented in this paper confirm the hypothesis based on femtosecond time-resolved absorption spectroscopy, as well as the results of molecular dynamics simulations, that heme doming is nearly complete on the sub-picosecond time scale under physiologically relevant conditions. The function of heme doming is to record the ultrafast chemical reaction of chemical bond rupture between the iron and the ligand, which allows the protein response to occur on a much longer time scale (Franzen et al., 1994b). The picture that emerges is an ultrafast chemical reaction of ligand dissociation (<50 fs) and heme doming (<700 fs), with concomitant rotation and tilt of the proximal histidine associated with a relatively small 0.15 Å movement of the F-helix (700 fs to at most 10 ps). We suggest that proximal histidine and tertiary F-helix displacement occur on a rapid time scale, on the basis of the available TRIR data and the sensitivity of the TRRR signal to changes in the tilt angle θ of the histidine. The rapidity of the protein response to the iron motion is important if the energy released by the out-of-plane motion is to be captured on the most rapid possible time scale in localized protein motions, which are crucial for the subsequent quaternary conformational changes in Hb. In the cooperative protein Hb, these are followed on the time scale of hundreds nanoseconds to microseconds by a 1 Å displacement of the F-helix (tertiary change) and contact formation between the FG corner of α and the C-helix of the corresponding β-subunit (quaternary change), as discussed elsewhere. Heme doming is the message that the chemical bond has been broken and does not in itself contain much of the free energy of cooperativity. The data presented confirm that heme doming is the primary event that gives rise to the transduction of the information of bond breaking into protein structural changes. This mechanism of transduction may also occur, for example, in cytochrome oxidase, which shows redox anti-cooperativity among the hemes (Babcock & Wikström, 1992). One hypothesis to account for the mechanism of anti-cooperativity among the two hemes of cytochrome oxidase involves a ligand switch hypothesis, in which it is the heme doming configuration that allows the redox state of one heme to be communicated to another (Woodruff et al., 1991) as part of a mechanism for proton pumping. The mechanism described here may function in other systems to translate ligand bond breakage and reformation into steric interactions among protein subunits.

REFERENCES

Agmon, N. (1988) *Biochemistry 27*, 3507−3511.

Ahmed, A. M., Campbell, B. F., Carusi, D., Chance, M. R., Chavez, M. D., Courtney, S. H., Friedman, J. M., Iben, I. E. T., Ondrias, M. R., & Yang, M. (1991) *Chem. Phys. 158*, 329−351.

Anfindrud, P. A., Han, C., & Hochstrasser, R. M. (1989) *Proc. Natl. Acad. Sci. U.S.A. 86*, 8387−8391.

Ansari, A., Berendzen, J., Bowne, S. F., Frauenfelder, H., Iben, I. E. T., Sauke, T. B., Shyamsunder, E., & Young, R. D. (1985) *Proc. Natl. Acad. Sci. U.S.A. 82*, 5000−5004.

Ansari, A., Jones, C. M., Henry, E. R., Hofrichter, J., & Eaton, W. A. (1992) *Science 256*, 1796−1798.

Argade, P. V., Sassaroli, M., Rousseau, D. L., Inubushi, T., Ikeda-Saito, M., & Lapidot, A. (1984) *J. Am. Chem. Soc. 106*, 6593−6596.

Armstrong, R. S., Irwin, M. J., & Wright, P. E. (1982) *J. Am. Chem. Soc. 104*, 626−627.

Asher, S. A., & Murtaugh, J. (1993) *J. Am. Chem. Soc. 105*, 7244−7251.

Austin, R. H., Roberson, M. W., & Mansky, P. (1989) *Phys. Rev. Lett. 62*, 1912−1915.

Babcock, G. T., & Wikström, M. (1992) *Nature 356*, 301−308.

Baldwin, J. M., & Chothia, C. (1979) *J. Mol. Biol. 129*, 175−220.

Bangcharoenpaurpong, O., Schomaker, K. T., & Champion, P. M. (1984) *J. Am. Chem. Soc. 106*, 5688−5698.

Bucci, E., & Fronticelli, C. (1965) *J. Biol. Chem. 240*, 551−553.

Campbell, B. F., Chance, M. R., & Friedman, J. M. (1987) *Science 238*, 373−376.

Causgrove, T. P., & Dyer, R. B. (1994) *Biochemistry* (in press).

Champion, P. M. (1988) in *Biological Applications of Raman Spectroscopy* (Spiro, T. G., Ed.) Vol. III, pp 262−290, Wiley & Sons, New York.

Chavez, M. D., Courtney, S. H., Chance, M. R., Kuila, D., Nocek, J., Hoffman, B. M., Friedman, J. M., & Ondrias, M. R. (1990) *Biochemistry 29*, 4844−4852.

Choi, S., & Spiro, T. G. (1983) *J. Am. Chem. Soc. 105*, 3683−3692.

Dasgupta, S., & Spiro, T. G. (1986) *Biochemistry 25*, 5941−5948.

Dasgupta, S., Spiro, T. G., Johnson, C. K., Dalickas, G. A., & Hochstrasser, R. M. (1985) *Biochemistry 24*, 5295−5297.

Dunn, R. C., & Simon, J. D. (1991) *Biophys. J. 60*, 884−889.

Eaton, W. A., Hanson, L. K., Stephens, P. J., Sutherland, J. C., & Dunn, J. B. R. (1978) *J. Am. Chem. Soc. 100*, 4991−5003.

Findsen, E. W., Friedman, J. M., Ondrias, M. R., & Simon, S. R. (1985a) *Science 229*, 661−664.

Findsen, E. W., Scott, T. W., Chance, M. R., Friedman, J. M., & Ondrias, M. R. (1985b) *J. Am. Chem. Soc. 107*, 3355−3357.

Findsen, E. W., Friedman, J. M., & Ondrias, M. R. (1988) *Biochemistry 27*, 8719−8724.

Franzen, S., Bohn, B., Poyart, C., & Martin, J.-L. (1994a) *J. Phys. Chem.* (submitted to M. El Sayed special issue).

Franzen, S., Lambry, J.-C., Bohn, B., Poyart, C., & Martin, J.-L. (1994b) *Nature Struct. Biol. 1*, 230−233.

Franzen, S., Bohn, B., Poyart, C., DePillis, G. D., Boxer, S. G., & Martin, J.-L. (1994c) *J. Biol. Chem.* (in press).

Friedman, J. M., & Campbell, B. F. (1987) in *Protein Structure: Molecular and Electronic Reactivity* (Austin, R., et al., Eds.) Springer, Berlin.

Friedman, J. M., Rousseau, D. L., & Ondrias, M. R. (1982a) *Annu. Rev. Phys. Chem. 33*, 471−491.

Friedman, J. M., Rousseau, D. L., Ondrias, M. R., & Stepnowski, R. A. (1982b) *Science 218*, 1244−1246.

Friedman, J. M., Campbell, B. F., & Noble, R. W. (1990) *Biophys. Chem. 37*, 43−59.

Gibson, Q. H., Regan, R., Elber, R., Olson, J. S., & Carver, T. E. (1992) *J. Biol. Chem. 267*, 22022−22034.

Gilch, H., Schweitzer-Stenner, R., & Dreybrodt, W. (1993) *Biophys. J. 65*, 1470−1485.

Henry, E. R., Levitt, M., & Eaton, W. A. (1985) *Proc. Natl. Acad. Sci. U.S.A. 82*, 2034−2038.

Hofrichter, J., Sommer, J. H., Henry, E. R., & Eaton, W. A. (1983) *Proc. Natl. Acad. Sci. U.S.A. 80*, 2235−2239.

Jackson, T. A., Lim, M., & Anfinrud, P. A. (1994) *Chem. Phys. 180*, 131−140.

Kitagawa, T., Nagai, K., & Tsubaki, M. (1979) *FEBS Lett. 104*, 376−378.

Kuczera, K., Kuriyan, J., & Karplus, M. (1990) *J. Mol. Biol. 213*, 351−362.

Kuriyan, J., Wilz, S., Karplus, M., & Petsko, G. A. (1986) *J. Mol. Biol. 192*, 133−154.

Lambright, D. G., Balasubramanian, S., & Boxer, S. G. (1991) *Chem. Phys. 158*, 249−260.

Li, X.-Y., & Zgierski, M. Z. (1992) *Chem. Phys. Lett. 188*, 16−20.

Li, P., Sage, J. T., & Champion, P. M. (1992) *J. Chem. Phys. 97*, 3214−3227.

Li, H., Elber, R., & Straub, J. E. *J. Biol. Chem.* (1993) *268*, 17908−17916.

Lim, M., Jackson, T. A., & Anfinrud, P. A. (1993) *Proc. Natl. Acad. Sci. U.S.A. 90*, 5801−5804.

Lingle, R., Jr., Xu, X., Zhu, H., Yu, S. C., & Hopkins, J. B. (1991) *J. Phys. Chem. 95*, 9320−9331.

Martin, J. L., Migus, A., Poyart, C., Lecarpentier, Y., Astier, R., & Antonetti, A. (1983a) *Proc. Natl. Acad. Sci. U.S.A. 80*, 173−177.

Martin, J. L., Migus, A., Poyart, C., Lecarpentier, Y., Astier, R., & Antonetti, A. (1983b) *EMBO J. 2*, 1815−1819.

Martin, J. L., Migus, A., Poyart, C., Lecarpentier, Y., Astier, R., & Antonetti, A. (1984) in *Ultrafast Phenomena IV* (Auston, D. H., & Eisenthal, K. B., Eds.) pp 447−451, Springer, Berlin.

Migus, A., Martin, J. L., Astier, R., & Orszag, A. (1980) in *Ultrafast Phenomena II* (Hochstrasser, R. M., et al., Eds.) pp 59−61, Springer, Berlin.

Monod, J., Wyman, J., & Changeux, J. P. (1965) *J. Mol. Biol. 12*, 88−118.

Myers, A. B., & Mathies, R. A. (1987) in *Biological Applications of Raman Spectroscopy* (Spiro, T. G., Ed.) Vol. II, pp 1−58, Wiley & Sons, New York.

Nagai, K., & Kitagawa, T. (1980) *Proc. Natl. Acad. Sci. U.S.A. 77*, 2033−2037.

Nienhaus, G. U., Mourant, J. R., & Frauenfelder, H. (1992) *Proc. Natl. Acad. Sci. U.S.A. 89*, 2902−2906.

Ondrias, M. R., Rousseau, D. L., & Simon, S. R. (1983) *J. Biol. Chem. 258*, 5638−5642.

Perutz, M. F. (1970) *Nature 228*, 726−739.

Perutz, M. F. (1979) *Annu. Rev. Biochem. 48*, 327−386.

Petrich, J. W., Martin, J. L., Houde, D., Poyart, C., & Orszag, A. (1987) *Biochemistry 26*, 7914−7923.

Petrich, J. W., Poyart, C., & Martin, J.-L. (1988) *Biochemistry 27*, 4049−4060.

Petrich, J. W., Lambry, J.-C., Kuczera, K., Karplus, M., Poyart, C., & Martin, J. L. (1991) *Biochemistry 30*, 3975−3987.

Richard, L., Genberg, L., Deak, J., Chiu, H.-L., & Miller, R. J. D. (1992) *Biochemistry 31*, 10703−10715.

Roder, H., Berendzen, J., Bowne, S. F., Frauenfelder, H., Sauke, T. B., Shyamsunder, E., & Weissman, M. B. (1984) *Proc. Natl. Acad. Sci. U.S.A. 81*, 2359−2363.

Rousseau, D. L., & Argade, P. V. (1986) *Proc. Natl. Acad. Sci. U.S.A. 83*, 1310−1314.

Saito, M., & Kashiwagi, H. (1985) *J. Chem. Phys. 82*, 3716−3721.

Sassaroli, M., & Rousseau, D. L. (1987) *Biochemistry 26*, 3092−3098.

Sassaroli, M., Dasgupta, S., & Rousseau, D. L. (1986) *J. Biol. Chem. 261*, 13704−13713.

Sawicki, C. A., & Gibson, Q. H. (1976) *J. Biol. Chem. 251*, 1533−1542.

Schaad, O., Zhou, H.-X., Szabo, A., Eaton, W. A., & Henry, E. R. (1993) *Proc. Natl. Acad. Sci. U.S.A. 90*, 9547−9551.

Scheidt, W. R., & Chipman, D. M. (1986) *J. Am. Chem. Soc. 108*, 1163−1167.

Scott, T. W., & Friedman, J. M. (1984) *J. Am. Chem. Soc. 106*, 5677−5687.

Spiro, T. G. (1988) in *Biological Applications of Raman Spectroscopy* (Spiro, T. G., Ed.) Vol. III, pp 1−37, Wiley & Sons, New York.

Srajer, V., & Champion, P. M. (1991) *Biochemistry 30*, 7390−7400.

Srajer, V., Schomaker, K. T., & Champion, P. M. (1986) *Phys. Rev. Lett. 57*, 1267−1270.

Stavrov, S. (1993) *Biophys. J. 65*, 1942−1950.

Stein, P., Terner, J., & Spiro, T. G. (1982) *J. Phys. Chem. 86*, 168−170.

Steinbach, P. J., Ansari, A., Berendzen, J., Braunstein, D., Chu, K., Cowen, B. R., Ehrenstein, D., Frauenfelder, H., Johnson, J. B., Lamb, D. C., Luck, S., Mourant, J. R., Nienhaus, G. U., Ormos, P., Philipp, R., Xie, A., & Young, R. D. (1991) *Biochemistry 30*, 3988−4001.

Tian, W. D., Sage, J. T., Srajer, V., & Champion, P. M. (1992) *Phys. Rev. Lett. 68*, 408−411.

Tsubaki, M., Srivastava, R. B., & Yu, N.-T. (1982) *Biochemistry 21*, 1132−1140.

van den Berg, R., & El-Sayed, M. A. (1990) *Biophys. J. 58*, 931−936.

Wells, A. V., Sage, J. T., Morikis, D., Champion, P. M., Chiu, M. L., & Sligar, S. G. (1991) *J. Am. Chem. Soc. 113*, 9655−9660.

Woodruff, W. H., Einarsottir, O., Dyer, R. B., Bagley, K., Palmer, G., Atherton, S. J., Goldbeck, R. A., Dawes, T. D., & Kliger, D. S. (1991) *Proc. Natl. Acad. Sci. U.S.A. 88*, 2588−2592.

Xie, X., & Simon, J. D. (1991) *Biochemistry 30*, 3682−3692.

Zhu, L., Li, P., Huang, M., Sage, J. T., & Champion, P. M. (1994) *Phys. Rev. Lett. 72*, 301−304.

BI9402580